

# DRY SLIDING WEAR BEHAVIOUR AND MICROSTRUCTURE OF THE W–Ni–Fe AND W–Ni–Cu HEAVY ALLOYS PRODUCED BY POWDER METALLURGY TECHNIQUE

M. Kilic,<sup>1</sup> D. Ozyurek,<sup>1,2</sup> and T. Tuncay<sup>1</sup>

UDC 621.762.96;5;669.275

*The effects of Fe and Cu on the wear behaviour of W–Ni alloys is investigated. W–Ni–Fe and W–Ni–Cu alloys are produced with six different compositions by the powder metallurgy technique. The microstructure is examined after shaping and sintering. Electron microscopy (SEM+EDS) and X-ray diffraction (XRD) are used to characterize the density, hardness, and grain size of W–Ni–Fe and W–Ni–Cu alloys produced by powder metallurgy technique. A pin-on-disc apparatus is used for the wear tests. All of the samples are tested under loads of 20 and 30 N, at a rate of 1 m/s and for five different sliding distances. It is found that, in Fe and Cu alloys, an increase in the W amount results in an increase in density and hardness. Furthermore, an increase in the W amount leads to a decrease in the amount of the binding phase for W–Ni–Fe and W–Ni–Cu alloys with a W content of 90, 93, and 97%, and results in reduced weight loss for W–Ni–Fe alloys.*

**Keywords:** tungsten heavy alloys, powder metallurgy, characterization, liquid phase sintering, wear behavior.

## INTRODUCTION

Tungsten heavy alloys (WHAs) are preferred in the production of parts that are subject to high temperatures and heavy wear damage. These alloys are commercial compounds, which contain 90–98% tungsten and have nickel–iron or nickel–copper compounds as a binding phase [1–5]. WHAs have superior properties: density of 17–18.5 g/cm<sup>3</sup>, hardness of 27–30 HRC, good machinability, corrosion and wear resistance, and low radioactive permeability [4]. For these reasons, tungsten is commonly used in: counter-weight and inertia kits in air platforms, race car cranks, medical equipment, armour and anti-piercing ammunition, sport equipments, and lead-free bullets that are used for hunting [6].

Tungsten has the highest melting temperature among metals. Therefore, it is necessary to produce tungsten alloys by powder metallurgy (PM) technique. It is possible to obtain the theoretical density through liquid phase sintering in the WHAs that are produced by PM technique [5, 7–10]. Provided that the theoretical density is achievable, these alloys have good machinability and ductile features [11]. Copper-containing alloys are preferred in the production of parts that have large cross-sections. Although these alloys have higher hardness compared to Fe-added W–Ni alloys, it is more difficult to sinter them to the full density. The most important advantage of copper-containing alloys is that they are not magnetic. The elemental metal powders in WHAs' can be mixed through any

<sup>1</sup>Karabuk University, Technology Faculty, Department of Manufacturing Engineering, Karabuk, Turkey.

<sup>2</sup>To whom correspondence should be addressed; e-mail: dozyurek@karabuk.edu.tr.

standard powder mixing method [12]. A cleaning procedure with hydrogen at approximately 1000°C is inserted into the process, no matter what the atmosphere is during sintering. For smaller parts, this procedure takes a few minutes, however, for larger parts, it can take more than an hour. Should the sintering be performed in vacuum, the cleaning procedure is applied throughout the whole sintering process. This procedure is important to keep the lubricants away and to get rid of the carbon remnants in the alloys shaped in a mould [13, 14].

In W–Ni–Fe alloys, the binding phase rate Ni/Fe must be within 1.5–4.0 in order to prevent brittle intermetallic phase formation. Mechanically weak phases ( $Fe_7W_6$ ) can be seen for Ni/Fe < 1.5, whereas intermetallic phases rich in nickel ( $Ni_4W$ ) are formed for Ni/Fe > 4. These intermetallic phases cannot be eliminated by secondary heat treatment. Earlier studies revealed that the formation of intermetallic phase is prevented, when the binding phase rate is 7/3, hence, the mechanical properties are improved [15, 16]. Therefore, the binding phase rate in the present study is selected to be 7/3.

The purpose of this study is to determine: (i) the effects of Fe and Cu on the microstructural properties, (ii) the wear behaviour of W–Ni alloys used in the defense industry, (iii) the element increasing wear resistance, (iv) compounds with the highest wear resistance, and (v) the mechanisms enhancing wear resistance.

### EXPERIMENTAL PROCEDURE AND MATERIALS

In this study, WHAs with high constant alloy element rates were produced by PM technique. Six different alloys were produced: W (90, 93, and 97%)–Ni–Fe and W (90, 93, and 97%)–Ni–Cu. The binding phase rate of the samples was 7/3. Table 1 lists the properties of the powders used, while Table 2 exhibits the alloy codes and the chemical composition of the alloys produced.

Figure 1 shows the SEM pictures of the W, Ni, Fe, and Cu starting powders, which demonstrate that the Fe, Cu, and Ni powders have spherical shape, while the W powder has a polygonal shape. In order to obtain the compositions given in Table 2, the elemental starting powders were weighed (wt.%) with a precision scale (1/10000) and then mixed in Turbula Shaker Mixer (Model T2F Glenn Mills) at 67 rpm for 45 min.

After mixing,  $\varnothing 12 \times (6-7)$  mm samples were prepared by cold-pressing the alloy powders using a 50-tons hydraulic press at a pressure of 600 MPa. Liquid phase sintering was carried out in two different groups: Fe alloy compositions and Cu alloy compositions [17]. The sintering was performed at 1000°C in pure  $H_2$  for 20 min and at 1480 and 1430°C in argon. During sintering of the Fe-added W–Ni alloys, the samples were heated to 1000°C with

TABLE 1. The Features of Powders Used in Experimental Studies

Properties	Powder (manufacturer)			
	Fe (W. Rowland Ltd.)	Cu (AEE)	Ni (AEE)	W (Eurotungstene)
Purity	99.5+	99.9+	99.9+	99.9+
Shape	Spherical	Spherical	Spherical	Poligonal
D10 ( $\mu m$ )	3.6	3.1	5.2	1.7
D50 ( $\mu m$ )	7.8	6.5	9.1	4.2
D90 ( $\mu m$ )	27.3	12.3	16.1	10.3

TABLE 1. Alloy Codes and Chemical Compositions of the Alloys Produced

Chemical composition, wt.%	Alloy code	Chemical composition, wt.%	Alloy code
90W–7Ni–3Fe	A1	90W–7Ni–3Cu	B1
93W–4.9Ni–2.1Fe	A2	93W–4.9Ni–2.1Cu	B2
97W–2.1Ni–0.9Fe	A3	97W–2.1Ni–0.9Cu	B3

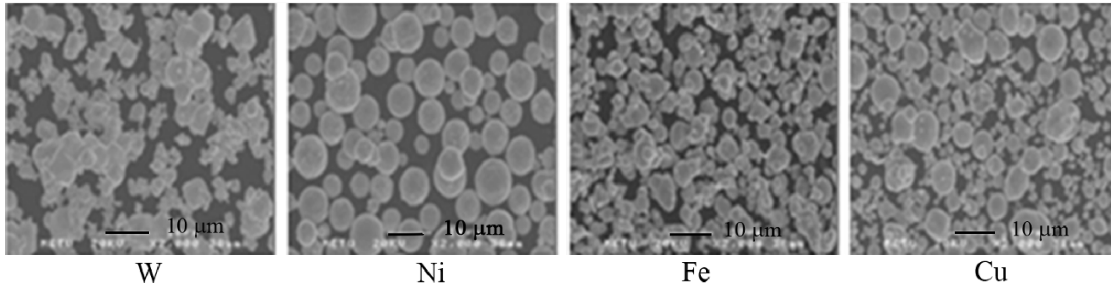


Fig. 1. SEM images of elemental powders used in experimental studies

a heating rate of 10°C/min, and after the oxide reduction at 1000°C in pure H<sub>2</sub> for 30 min, they were heated to 1480°C with a heating rate of 3°C/min. After sintering at 1480°C, the samples were cooled in a furnace in pure H<sub>2</sub> and in argon for 20 and 10 min, respectively. During sintering of Cu-added W–Ni alloys, the samples were heated to 1000°C with a heating rate of 10°C/min. After oxide reduction at 1000°C in pure H<sub>2</sub> for 30 min, they were heated to 1430°C with a heating rate of 3°C/min. After sintering at 1430°C in pure H<sub>2</sub> and in argon for 20 and 10 min, respectively, the samples were cooled in a furnace.

After the surfaces of the sintered samples were prepared with metallographic processes, they were etched with a mixture of 2 mL (HF), 90 mL pure water, 5 mL (HNO<sub>3</sub>), and 3 mL (HCl) reactive agent for 30–45 sec for microstructural examinations. The density of the seven samples was measured according to Archimedes' principle and these measurements were then averaged. Furthermore, the hardness of the samples was measured by using an Affri System VRSD-251 universal macrohardness tester (HRC). Five hardness tests were carried out for each sample and the hardness values were then averaged.

To conduct wear tests, a pin-on-disc apparatus (that can operate with any load, at any sliding speed, and at any revolution rate) was used. The metallographic processing with a 1200-grid sandpaper and polishing with a 6-μm diamond paste allowed obtaining the same surface quality for each sample. The disc and the sample surfaces were cleaned with acetone before testing. Dry sliding wear tests were carried out using a standart pin-on-disc apparatus with a continuously rotating alloy steel plate (AISI 4140) of hardness 60–64 HRC that acted as a counter surface. The wear tests were conducted under the following conditions: 20 and 30 N loads, five different sliding distances (600, 1200, 1800, 2400, and 3000 m), and a sliding speed of 1 m · sec<sup>-1</sup> [18]. The worn samples were later weighted on a precision scale (1/10000) and the weight loss was determined using Eq. (1) [19]:

$$W_a = \frac{\Delta G(\text{mg})}{d \cdot P \cdot S(\text{g/cm}^3 \cdot \text{N} \cdot \text{m})}, \quad (1)$$

where  $W_a$  is the wear rate, mm<sup>3</sup>/N · m;  $\Delta G$  is the weight loss, mg;  $P$  is the load, N;  $S$  is the sliding distance, m;  $d$  is the density, g/cm<sup>3</sup>. A JEOL JSM-6400 scanning electron microscope (SEM+EDS) was used to examine the microstructure. Moreover, the wear surfaces and the wear powders of the samples were examined with SEM. The grain size measurement was carried out according to Jeffries method illustrated in ASTM Standard E 112-96:

$$N_A = f(N_{\text{inside}} + N_{\text{intercepted}}/2), \quad (2)$$

$$G = (3.321928 \log_{10} N_A) - 2.954, \quad (3)$$

where  $N_A$  is the grain count per 1 mm<sup>2</sup>;  $N_{\text{inside}}$  is the grain size in a circle of 5000 mm<sup>2</sup> (Ø79.8 mm) on a 100 × 100 mm SEM image, mm<sup>4</sup>;  $N_{\text{intercepted}}$  is the grain count that the circle intersects. The value of  $G$  is found from Eq. 3 by multiplying the function with the coefficient given in the size scale of the image. To determine the phases formed in the structure during sintering, XRD tests were performed using a GE Seifert XRD-3003-PTS. The measurement was carried out under the following conditions: copper (Cu) $K_{\alpha}$ , voltage of 40 kV, current of 45 mA, measurement speed of 1°/102 sec, and angle range of 35–120°.

## RESULTS AND DISCUSSION

*Microstructural Characterization.* Figure 2 depicts the scanning electron microscope (SEM) images of W–Ni–Cu and W–Ni–Fe alloys produced by PM technique. According to these images, the matrix and the binding phase have a homogeneous distribution throughout the alloy structure for all of the alloy groups. During the liquid phase sintering, W grain growth occurs. Dissolved tungsten atoms diffuse into the liquid phase or into the larger tungsten grains and cause them to grow.

Table 3 lists the energy dispersive spectroscopy (EDS) results. These results suggest that the dissolution rate of tungsten in the liquid phase of W–Ni–Fe and W–Ni–Cu alloys is approximately 9.6–11 at.%. However, the tungsten dissolution rate in the liquid phase of 97W–2.1Ni–0.9Cu (B3) alloy is 4.2 at.%.

Figure 3 shows the XRD results of W–Ni–Fe and W–Ni–Cu alloys. According to these results, the  $\text{Fe}_3\text{Ni}_2$  phase is formed along the grain boundaries of 90W–7Ni–3Fe (A1) alloy. In the structures of 93W–4.9Ni–2.1Fe (A2) alloy and 97W–2.1Ni–0.9Fe (A3) alloy,  $\text{Fe}_{0.64}\text{Ni}_{0.36}$ ,  $\text{Ni}_{17}\text{W}_3$ ,  $\text{Cu}_{0.4}\text{W}_{0.6}$ , and  $\text{Ni}_{17}\text{W}_3$  phases are formed in the structure of W–Ni–Cu alloys. Earlier study revealed that it needs to be  $1.5 < \text{Ni/Fe/Cu} < 4$  in order to prevent the possible brittle intermetallic phases formed during liquid phase sintering in the alloy structure [16]. Figure 3 shows that these possible brittle intermetallic phases formed during liquid phase sintering in the alloy structure (such as  $\text{Fe}_7\text{W}_6$  and  $\text{Ni}_4\text{W}$ ) were not formed.

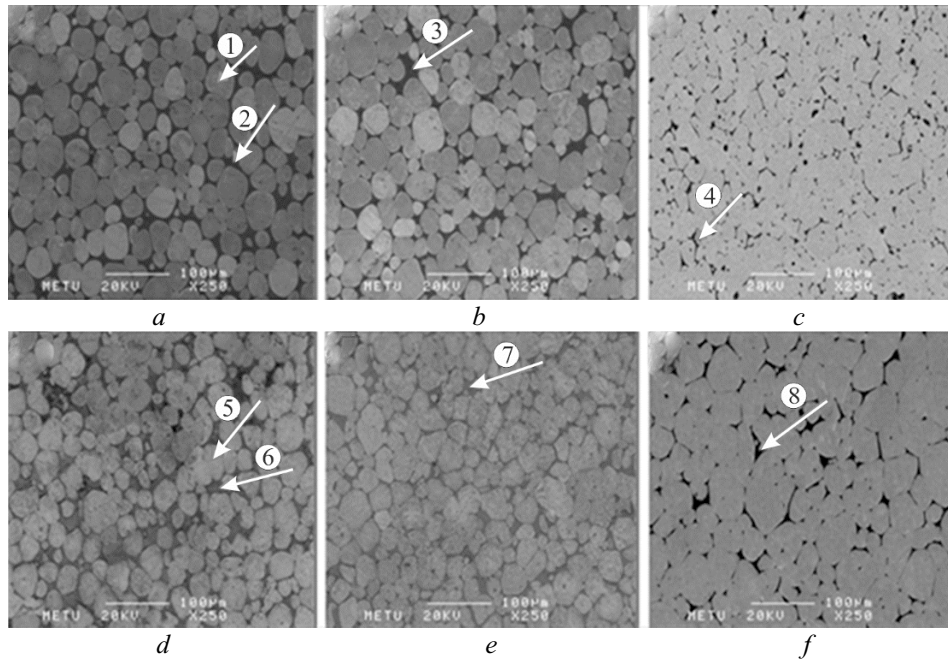


Fig. 2. SEM images of W–Ni–Cu and W–Ni–Fe alloys

TABLE 3. Results of Electron Dispersive Spectroscopy (in at.%)

Figure	Location	W	Ni	Fe	Cu
2a	1	100	–	–	–
2a	2	11.01	61.85	27.14	–
2b	3	9.59	62.48	27.93	–
2c	4	10.85	64.05	25.10	–
2d	5	100	–	–	–
2d	6	10.34	70.68	–	18.98
2e	7	11.62	69.10	–	19.28
2f	8	4.26	74.23	–	21.51

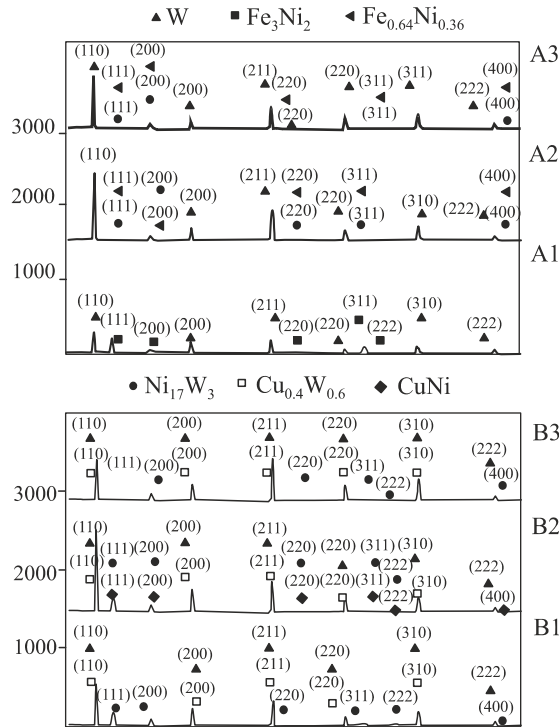


Fig. 3. XRD results of W–Ni–Fe and W–Ni–Cu alloys

Figure 4 shows the density and hardness changes in the W–Ni–Cu and W–Ni–Fe alloys produced by the powder metallurgy method. Figure 4a demonstrates that increasing the amount of W increases the density. When the measured density values are compared with those given in ASTM Standard B 777-07, it can be seen that 99% of the theoretical density was obtained in 90W–7Ni–3Fe (A1) and 97W–2.1Ni–0.9Cu (B3) alloys. In 97W–2.1Ni–0.9Fe (A3) and 90W–7Ni–3Cu (B1) alloys, the theoretical density is in the determined range. The reason behind the increase in density is that the W density of the alloy is higher (19.3 g/cm<sup>3</sup>) than that of other alloying elements. Therefore, the higher the amount of W in the alloy the higher the density of the alloy. The density of 93W–4.9Ni–2.1Fe (A2) and 93W–4.9Ni–2.1Cu (B2) alloys, which have no match in the standard, is found to be higher than that of the samples produced in the study conducted by Islam et al. [20], which had the same compound and a density of 17.52 g/cm<sup>3</sup>.

Hardness tests were carried out on 3 samples with the highest density. Five measurements were carried out on each sample in order to find the average hardness. According to the hardness results (Fig. 4b), an increase in tungsten amount in the alloys that have Ni–Fe as binding phase resulted in an increase in hardness. However, in the alloys that have Ni–Cu as binding phase, it was seen that an increase in tungsten amount did not result in a linear increase in hardness, and the values were very close to each other.

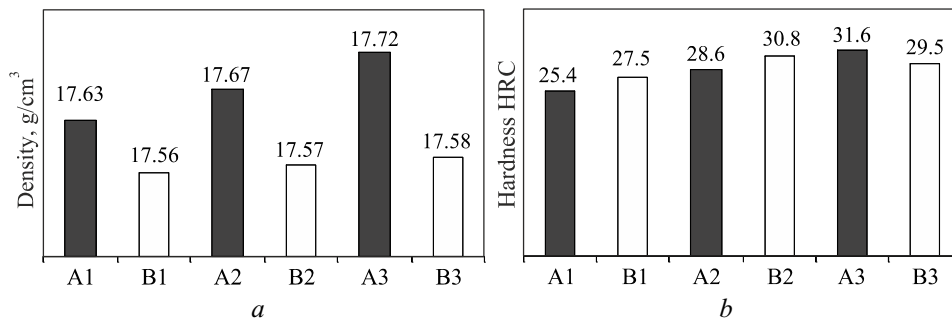


Fig. 4. Density and hardness changes of W–Ni–Cu and W–Ni–Fe alloys

Moreover, it was found that  $\text{Ni}_{17}\text{W}_3$  phase count formed in the structure of 97W–2.1Ni–0.9Cu (B3) alloy was very low compared to the other alloys. This explains the fact that 97W–2.1Ni–0.9Cu (B3) alloy has a lower hardness than 93W–4.9Ni–2.1Cu (B2) alloy. The lower count of this phase results in a lower hardness. Correlating the decrease in hardness of 97W–2.1Ni–0.9Cu (B3) alloy composition with the EDS results shows that W dissolution in the binding phase is low (Table 3). SEM images (Fig. 2) demonstrate that, in the samples with increased tungsten amount, the amount of the binding phase is also low and the grains are very close to each other. The low amount of binding phase around tungsten grains results in a growth in grain size because of the high sintering temperature. Grain size measurements were carried out in order to determine the relation between the grain size, microstructure, and hardness in WHAs. The grain size measurements were carried out according to Jeffries method (Eqs. (2) and (3)). Figure 5 shows the results of grain size measurements.

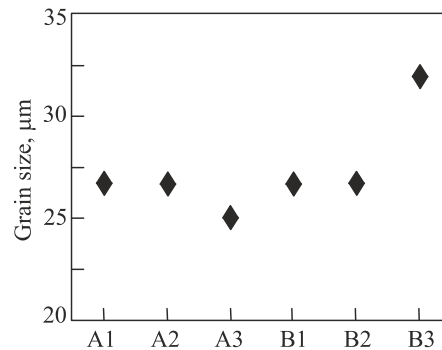


Fig. 5. Grain size changes in W–Ni–Cu and W–Ni–Fe alloys

According to the results of grain size measurements (Fig. 5), the average grain size of 90W–7Ni–3Fe (A1) and 93W–4.9Ni–2.1Fe (A2) alloys, 90W–7Ni–3Cu (B1) and 93W–4.9Ni–2.1Cu (B2) alloys was 26.7  $\mu\text{m}$ . In a study conducted by Mondal et al. [16], 90W–7Ni–3Fe (A1) samples had an average grain size of 26  $\mu\text{m}$ . This result is close to the grain size of 90W–7Ni–3Fe (A1) alloy, which has the same composition and a grain size of 26.7  $\mu\text{m}$ . The average grain size of 97W–2.1Ni–0.9Fe (A3) and 97W–2.1Ni–0.9Cu (B3) alloys was 25  $\mu\text{m}$  and 31.8  $\mu\text{m}$ , respectively. Although 97W–2.1Ni–0.9Fe (A3) alloy has a very similar grain size (compared to other alloys), a growth of the grain size in 97W–2.1Ni–0.9Cu (B3) alloy was observed. The lower hardness of 97W–2.1Ni–0.9Cu (B3) alloy compared to 93W–4.9Ni–2.1Cu (B2) alloy is due to the larger grain size. Since the desired density and hardness was not reachable during sintering at 1430°C, the sintering of 97W–2.1Ni–0.9Cu (B3) alloy was repeated at 1480°C. There was an improvement in terms of density, but still the desired hardness was not reached. Belhadjhamida and German [21] have pointed out that the tungsten grain size and distribution in WHAs is related to the sintering time and temperature. Therefore, a growth in grain size occurred in 97W–2.1Ni–0.9Cu (B3) alloy. The grain growth occurs because of the higher diffusion rate between grains as a result of the increase in the sintering temperature.

*Dry Sliding Wear Tests.* The material hardness is an important factor for friction and wear. Therefore, the material hardness cannot be ignored when determining the mechanical and wear behaviour of material. It is a metallurgical fact that the higher the material hardness, the higher the material resistance [22–24]. The results of this study are in accordance with this fact. Figure 6 depicts the dry sliding wear test results regarding the weight loss and the friction coefficient of W–Ni–Fe (A1–A2–A3) and the W–Ni–Cu (B1–B2–B3) alloys as a function of the applied 20 and 30 N loads and the sliding distance.

It can be seen that an increase in the tungsten content led to a decrease in the weight loss. When the weight loss is linked to the density and hardness (Fig. 4), it can be observed that the higher the density and the hardness, the lower the weight loss. Moreover, when the weight loss is linked to the EDS results (Table 3), the highest weight loss is observed for 90W–7Ni–3Fe (A1) alloy, which has the highest amount of binding phase. In other words, the higher the binding phase amount, the higher the weight loss. This is due to the increase in the wear resistance.

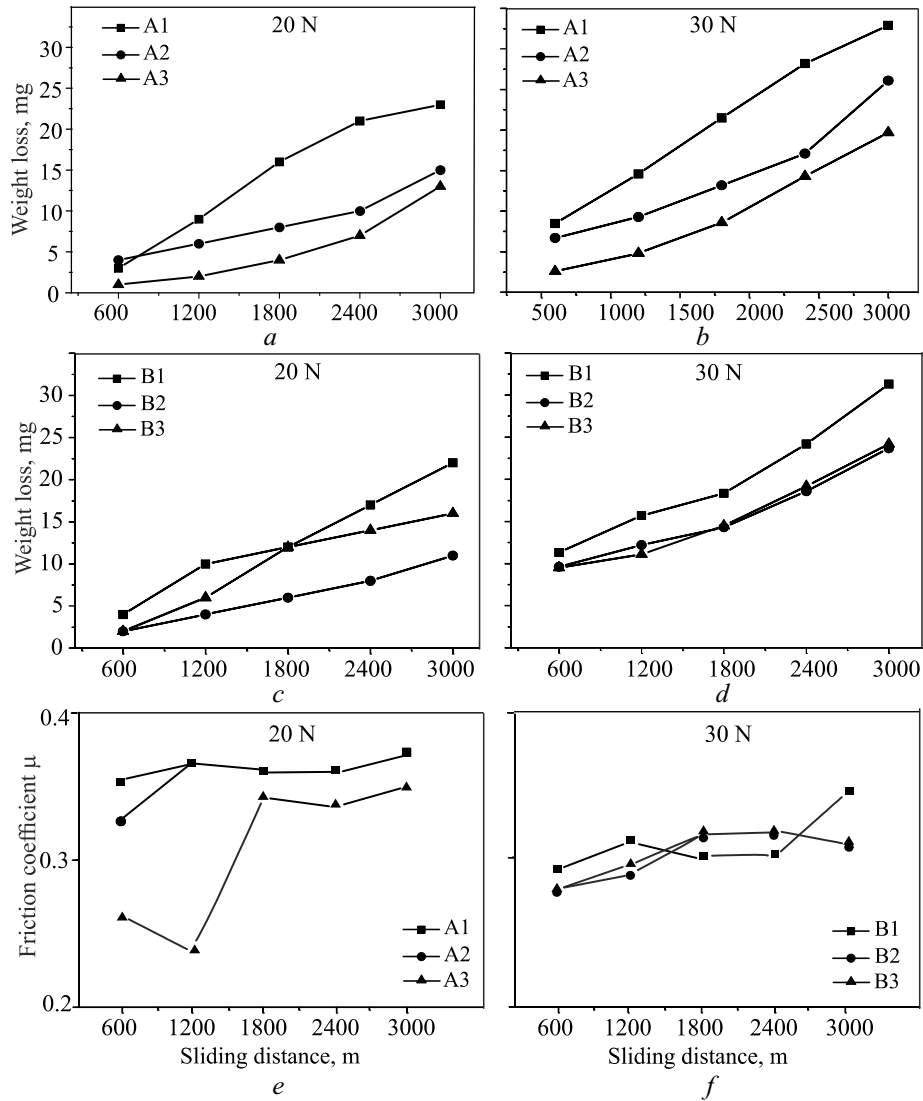


Fig. 6. Weight loss and friction coefficient of W–Ni–Fe (A1–A2–A3) and W–Ni–Cu (B1–B2–B3) alloys tested under 20 and 30 N loads

When the dry sliding wear test results of W–Ni–Cu (B1–B2–B3) alloys (Fig. 6) are examined, at the end of the sliding distance of 3000 m, 90W–7Ni–3Cu (B1) alloy has the highest weight loss, while 93W–4.9Ni–2.1Cu (B2) and 97W–2.1Ni–0.9Cu (B3) alloys have very similar weight loss. This is due to the fact that 97W–2.1Ni–0.9Cu (B3) alloy has lower hardness than 93W–4.9Ni–2.1Cu (B2) alloy. In addition, it is thought that the low tungsten solubility of the binding phase in 97W–2.1Ni–0.9Cu (B3) alloy increases the weight loss. This implies the idea that the matrix phase amount dissolved in the binding phase has a negative effect on the wear behaviour. Another important factor that increases the weight loss is that this alloy has a larger grain size, compared to the other alloys.

When the applied load is increased from 20 to 30 N during wear tests, it is seen that the weight loss also increases (Fig. 6). Especially, during the wear tests carried out under 20 N load, while significant weight loss of 93W–4.9Ni–2.1Cu and 97W–2.1Ni–0.9Cu alloy is observed. However, weight loss decreases when the applied load is 30 N.

The higher weight loss under 20 N could be attributed to the fractures during dry sliding. Fractures of PM-produced components are reported in the previous studies [25, 26].

According to Figure 6, 97W–2.1Ni–0.9Fe (A3) alloy manifests the highest increase in the friction coefficient value at the end of the sliding distance of 3000 m, whereas 90W–7Ni–3Fe (A1) alloy shows the lowest



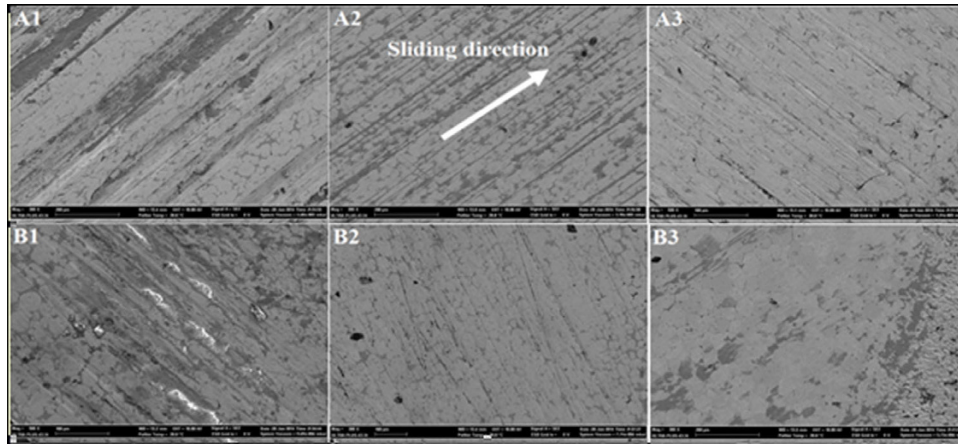


Fig. 7. SEM images of worn surfaces of W-Ni-Fe (A1-A2-A3) and W-Ni-Cu (B1-B2-B3) alloys

increase. However, at the end of the sliding distances of 1200, 1800, 2400, and 3000 m, while 90W-7Ni-3Fe (A1) and 93W-4.9Ni-2.1Fe (A2) alloys have almost identical friction coefficients, 97W-2.1Ni-0.9Fe (A3) alloy, which experiences the least weight loss, has a lower friction coefficient. Given the weight loss, 93W-4.9Ni-2.1Fe (A2) alloy was expected to have a higher friction coefficient than 90W-7Ni-3Fe(A1) alloy. Nevertheless, at the end of

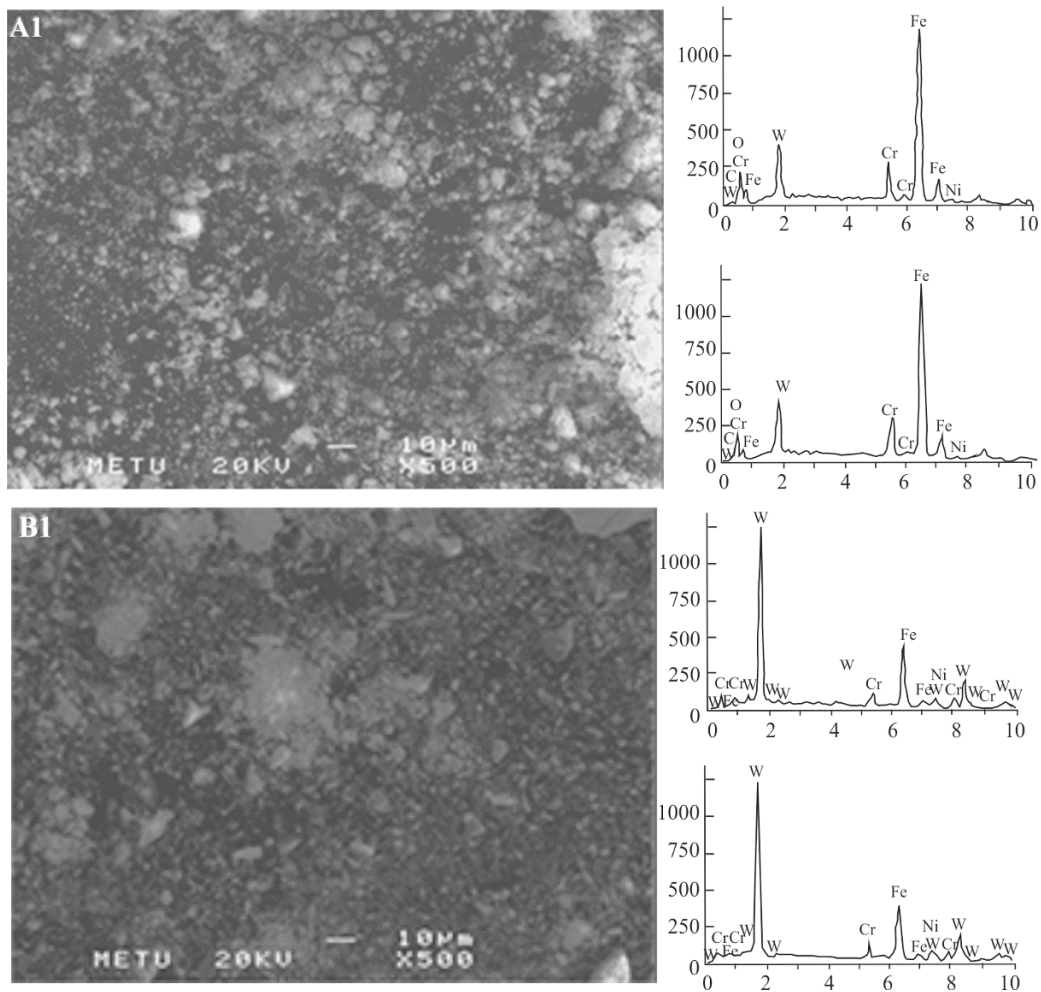


Fig. 8. SEM images and EDS results of the wear tests of the powders of 90W-7Ni-3Fe (A1) and 90W-Ni-3Cu (B1) alloys



the sliding distance of 600 m, the friction coefficients suggest that the reverse is true. This is because the small particles leaving the surface of 90W–7Ni–3Fe (A1) alloy were stuck between the sample and abrasive disc and got attached to the surface of the sample. As a result of the sliding process, these smaller particles get attached to the other parts of the surface and narrow the pin–disc contact surface, leading to an increase in the friction coefficient value. However, the friction coefficients observed after 600 m were as expected. According to Figure 6, the friction coefficients achieved after 600, 1200, 1800, 2400, and 3000 m satisfy the relationship  $B1 > B2 \approx B3$  for W–Ni–Cu alloys, thus, the friction coefficients are in accordance with the weight losses.

Figure 7 shows the SEM images of the worn surfaces of W–Ni–Fe (A1–A2–A3) and the W–Ni–Cu (B1–B2–B3) alloys under 20 N load and at the end of the sliding distance of 3000 m. Wear tracks in the sliding direction on the worn surface of 90W–7Ni–3Fe (A1) alloy are observed. Moreover, a partial adhesion caused by the small particles mentioned above is also visible on the worn surface. The sliding direction and the wear track on 93W–4.9Ni–2.1Fe (A2) and 97W–2.1Ni–0.9Fe (A3) alloys are very visible. During the wear tests, an oxidation (white areas) occurred on the surface of 90W–7Ni–3Cu (B1) alloy. For 93W–4.9Ni–2.1Cu (B2) alloy, the sliding direction is visible, while the wear tracks are not very visible. On the other hand, for 97W–2.1Ni–0.9Cu (B3) alloy, the sliding direction and the wear tracks are not visible at all.

Figure 8 depicts the SEM images and the EDS results of the dry sliding wear tests. The EDS analysis of the worn powders of 90W–7Ni–3Fe (A1) alloy was performed at two different spots. It was found that the powders consisted of Cr (12.63 at.%), Fe (80.13 at.%), Ni (1.94 at.%), and W (5.29 at.%). The Cr and Fe powders were produced by the abrasion on the abrasive disk during the wear tests. Moreover, it is thought that a part of the Fe phase came from the binding phase. On the other hand, the EDS analysis of 90W–7Ni–3Cu (B1) alloy suggests that the powders consisted of Cr (8.90 at.%), Fe (44.76 at.%), Ni (7.88 at.%), W (27.99 at.%), and Cu (10.57 at.%).

## CONCLUSIONS

Dry sliding wear behaviour of W–Ni–Fe and W–Ni–Cu alloys produced by the PM technique has been investigated and the following observations have been made:

- An increase in the tungsten content leads to an increase in the density of the samples, which have Ni–Fe and Ni–Cu as binding phases with a W content of 90, 93, and 97%.
- In the samples, which have Ni–Fe as a binding alloy, an increase in the tungsten content leads to an increase in hardness. In the samples, which have Ni–Cu as binding phases, increasing the tungsten content from 90 to 93% increases the hardness of the samples, while increasing the tungsten content from 93 to 97% causes the hardness to decrease.
- In W–Ni–Fe and W–Ni–Cu alloys with a W content of 90, 93, and 97%, an increase in the tungsten content leads to a decrease in the amount of the binding phase.
- The average grain size of A1, A2, B1, and B2 alloys is 26.7  $\mu\text{m}$ , while A3 and B3 alloys have a grain size of 25 and 31.8  $\mu\text{m}$ , respectively.
- During dry sliding wear tests of W–Ni–Fe alloys, an increase in the tungsten content leads to a decrease in the weight loss.
- The A3 alloy has the lowest friction coefficient among all of W–Ni–Fe alloys, while B2 alloy has the lowest friction coefficient among all of W–Ni–Cu alloys.

## REFERENCES

1. C. L. Chen and C. L. Huang, “Milling media and alloying effects on synthesis and characteristics of mechanically alloyed ODS heavy tungsten alloys,” *Int. J. Refract. Met. Hard Mater.*, **44**, 19–26 (2014).
2. Y. Jin, S. Cao, J. Zhu, et al., “Gradient structure induced by molybdenum in 90W–Ni–Fe heavy alloy,” *Int. J. Refract. Met. Hard Mater.*, **43**, 141–146 (2014).
3. H. J. Ryu, S. H. Hong, and W. H. Baek, “Microstructure and mechanical properties of mechanically alloyed and solid state sintered tungsten heavy alloys,” *Mater. Sci. Eng. A*, **291**, 91–96 (2000).
4. S. G. Caldwell, “Heat Treatment of tungsten alloys,” *Int. Powder Metall.*, **39**, No. 7, 43–51 (2003).

5. S. J. Park, J. L. Johnson, Y. Wu, et al., "Analysis of the effect of solubility on the densification behaviour of tungsten heavy alloys using the master sintering curve approach," *Int. J. Refract. Met. Hard Mater.*, **37**, 52–59 (2013).
6. L. Ding, D. P. Xiang, Y. Y. Li, et al., "Effects of sintering temperature on fine-grained tungsten heavy alloy produced by high-energy ball milling assisted spark plasma sintering," *Int. J. Refract. Met. Hard Mater.*, **33**, 65–69 (2012).
7. H. Ibrahim, A. Aziz, and A. Rahmat, "Enhanced liquid-phase sintering of W–Cu composites by liquid infiltration," *Int. J. Refract. Met. Hard Mater.*, **43**, 222–226 (2014).
8. H. Liu, S. Cao, J. Zhu, et al., "Densification, microstructure and mechanical properties of 90W–4Ni–6Mn heavy alloy," *Int. J. Refract. Met. Hard Mater.*, **37**, 121–126 (2013).
9. J. Zhu, S. Cao, and H. Liu, "Fabrication of W–Ni–Fe alloys gradient structures", *Int. J. Refract. Met. Hard Mater.*, **36**, 72–75 (2013).
10. N. K. Caliskan, N. Durlu, and S. Bor, "Swaging of liquid phase sintered 90W–7Ni–3Fe tungsten heavy alloy," *Int. J. Refract. Met. Hard Mater.*, **36**, 260–264 (2013).
11. J. W. Noh, E. P. Kim, H. S. Song, et al., "Matrix penetration of W–W grain-boundaries and its effect on mechanical properties of 93W–5.6Ni–1.4Fe heavy alloys," *Metall. Trans. A*, **24**, No. 11, 2411–2416 (1993).
12. J. J. Dunkley, *Powder Metallurgy, Metal Handbook*, ASM International Publ., **7**, No. 9, 111–112 (1998).
13. A. Upadhyaya, "Processing strategy for consolidation tungsten heavy alloys for ordnance applications," *Mater. Chem. Phys.*, **67**, 101–110 (2001).
14. S. H. Hong and H. D. Ryu, "Combination of mechanical alloying and two-stage sintering of 93W–5.6Ni–1.4Fe tungsten heavy alloy," *Mater. Sci. Eng. A*, **344**, 253–260 (2003).
15. J. Liu and R. M. German, "Rearrangement densification in liquid-phase sintering," *Metall. Mater. Trans. A*, **32**, 3125–3131 (2001).
16. A. Mondal, A. Upadhyaya, D. Agrawal, "Effect of heating mode and sintering temperature on the consolidation of 90W–7Ni–3Fe alloys," *J. Alloy Compd.*, **509**, 301–310 (2011).
17. R. M. German, *Sintering Theory and Practice*, John Wiley and Sons, Inc., New York (1996), pp. 169–170.
18. M. Kilic, *An Investigation of the Effects of Cu and Fe Addition on Wear Behaviour of Tungsten Alloys*, M.Sc. Thesis, Karabuk Univ. (2013).
19. R. M. German, S. C. Farooq, and M. Kipphut, "Kinetics of liquid phase sintering," *Mater. Sci. Eng. A*, 105/106, 215–224 (1998).
20. S. H. Islam, F. Akhtar, S. J. Askari, et al., "Tensile behavior change depending on the varying tungsten content of W–Ni–Fe alloys," *Int. J. Refract. Met. Hard Mater.*, **25**, 380–385 (2007).
21. A. Belhadjhamida and R. M. German, "Tungsten and tungsten alloys by powder metallurgy," (*Annual Meeting and Exhibition of the Minerals, Metals, and Materials Society (TMS); New Orleans, LA (United States); 17–21 Feb., 1991*), TMS, Warrendale, USA (1991), pp. 3–19.
22. D. Özyürek, M. Yildirim, I. Ciftci, "The tribological properties of A356–SiC<sub>p</sub> metal-matrix composites fabricated by thixomoulding technique," *Sci. Eng. Compos. Mater.*, **19**, No. 4, 351–356 (2012).
23. D. Özyürek and I. Ciftci, "An Investigation into wear behaviour of TiB<sub>2</sub> particle reinforced aluminum composites produced by mechanical alloying," *Sci. Eng. Compos. Mater.*, **18**, No. 1–2, 5–12 (2011).
24. D. Özyürek, S. Tekeli, A. Güral, et al., "Effect of Al<sub>2</sub>O<sub>3</sub> amount on microstructure and wear properties of Al–Al<sub>2</sub>O<sub>3</sub> metal matrix composites prepared using mechanical alloying method," *Powder Metall. Met. Ceramics*, **49**, Nos. 5–6, 289–294 (2010).
25. A. Güral, S. Tekeli, D. Özyürek, and M. Gürü, "Effect of repeated quenching heat treatment on microstructure and dry sliding wear behavior of low carbon PM steel," *Mater. Sci. Forum*, **534–536**, 673–676 (2007).
26. D. Özyürek, S. Tekeli, T. Tuncay, and R. Yilmaz, "Exchange of experience the effect of synthesis time on the wear behavior of Al–8%Ti alloy produced by mechanical alloying," *Powder Metall. Met. Ceramics*, **51**, Nos. 7–8, 481–495 (2012).